Asian Journal of Chemistry; Vol. 35, No. 5 (2023), 1079-1088

ASIAN JOURNAL OF CHEMISTRY

https://doi.org/10.14233/ajchem.2023.27711

Synthesis, Electrochemical, Morphological, Computational and Corrosion Inhibition Studies of 3-(5-Naphthalen-2-yl-[1,3,4]oxadiazol-2-yl)-pyridine against Mild Steel in 1 M HCl

DEEPAK SHARMA[1], ABHINAY THAKUR[2], MANISH KUMAR SHARMA[1], KRANTI JAKHAR[1], ASHISH KUMAR[3], ASHOK KUMAR SHARMA[1,*] and HARI OM[1,*]

[1]Department of Chemistry, Deenbandhu Chhotu Ram University of Science & Technology, Murthal-131039, India
[2]Department of Chemistry, School of Chemical Engineering and Physical Sciences, Lovely Professional University, Phagwara-144402, India
[3]Department of Science and Technology, Nalanda College of Engineering, Nalanda-803101, India

*Corresponding authors: E-mail: draksharma.chem@dcrustm.org; hariom.chem@dcrustm.org

Received: 20 February 2023; *Accepted*: 25 March 2023; *Published online*: 28 April 2023; AJC-21213

1,3,4-Oxadiazole derivative, namely, 3-(5-naphthalen-2-yl-[1,3,4]oxadiazol-2-yl)pyridine (NOP) as a corrosion inhibitor against mild steel in 1M HCl has been evaluated using the weight-loss technique (303-323 K), electrochemical analysis [potentiodynamic polarization (PDP) and electrochemical impedance spectroscopy (EIS)], as well as surface morphology investigations (SEM). Additionally the computational studies such as density functional theory (DFT), the synthesized molecule (NOP) were utilized to better insight into molecular structure and electronic aspects relating to the anti-corrosion activities of the examined inhibitors and to envisage the interaction between designed inhibitors with the mild steel surface. The synthesized molecule (NOP) expressed high inhibition efficiency of 88.62% at an optimal concentration of 500 ppm at 298 K. A mixed-type inhibition mechanism is suggested by potentiodynamic polarization (PDP) analysis. The DFT calculations complement well with the experimental outcomes. This article provides in-depth insights to comprehend the mild steel inhibitor interactions mode and can be very helpful in accentuating the approach to mitigate the metal dissolution occurring in acidic corrosive media.

Keywords: Corrosion, Mild steel, 1,3,4-Oxadiazole derivatives, Synthesis, Adsorption, Electrochemical impedance spectroscopy.

INTRODUCTION

Since the discovery of metals, mild steel has garnered substantial interest due to its outstanding engineering characteristics, including its lower cost, ease of availability and significant mechanical strength (flexibility, strength, malleability, among others) [1-3]. Despite these potentials, one of the main issues with mild steel is its propensity to corrode when acidic solutions are present nearby in several processes, including acid cleaning, acid pickling, descaling and oil well acidizing. This fastens the deterioration rate of mild steel in a large extent [4-7]. Additionally, in specific industries, several inorganic and organic chemicals dissolved in pipeline oil hasten the corrosion of mild steel [8,9]. As a result, it is essential to consider the developments in engineering and chemical formulations that can trigger the corrosion rate and reduce the catastrophic incidents induced by metallic corrosion.

Over the past few decades, researchers have emphasized effective strategies for mitigating metal corrosion by using eco-friendly corrosion inhibitors, cathodic and anodic protection approaches and material selection [10-13]. These corrosion inhibitor formulations are utilized in small amounts to lessen the environmental damage caused by interfering with the anodic and/or cathodic reaction or slowing the oxidation process. The inhibition efficacy of the organic molecules depends upon various parameters such as the accessibility of adsorption sites, the metal's characteristics, modes of interaction, the shape of the molecule and the experimental conditions such as pH, immersion time and temperature. They must also be capable of adhering to metal surfaces to develop a defensive barrier [14,15]. Most organic inhibitors adsorb to metallic surfaces *via* heteroatoms enriched with π- and unshared electron pairs. The effectiveness of the inhibitors is also influenced by the donor atoms' size, electron density and orbital properties, among others [16,17].

The N- and O-containing organic heterocyclic compounds have been the subject of substantial research among the various organic compounds. They have considerable adsorption tendency, forming a dense defensive layer on the metallic substrate.

1,2,3-Triazoles, 1,2,4-triazoles, 1,2,4-triazines, pyrazoles, benzimidazoles, thiazoles and oxadiazoles find prominent place among the popular organic corrosion inhibitors [18,19]. Oxadiazoles are getting popular in multiple applications owing to their low toxicity, environmental friendliness and biodegradability [20-24]. Because of the aromatic ring's electron density, N and O atoms exhibit a distinctive interaction with the Fe *d*-orbital, quickly erecting a barrier on the metallic surface. Oxadiazoles have an intriguing affinity for metal surfaces and can more easily remove the water molecules adsorbed on the metal surfaces than other traditional corrosion inhibitors.

In this study, a novel and environmentally friendly 3-(5-naphthalen-2-yl-[1,3,4]oxadiazol-2-yl)-pyridine (NOP) is synthesized to mitigate the corrosion rate of mild steel in robust corrosive environments (1M HCl). The electrochemical measurements, weight loss and SEM techniques were utilized to examine the effectiveness of corrosion inhibition and the interaction between the mild steel and synthesized molecule (NOP) in 1M HCl. Furthermore, the DFT analysis was also computed to correlate the experimental outcomes with the theoretical data.

EXPERIMENTAL

Preparation of solutions: The acid electrolyte was prepared using analytical grade 37% HCl (ρ = 1.18 g/mL). Stock solution of the synthesized novel oxadiazole dertivative *viz*. 3-(5-naphthalen-2-yl-[1,3,4]oxadiazol-2-yl)pyridine (NOP) was obtained in 1M HCl solution by serial dilution method and its concentration was employed from 50-500 ppm. For each experiment, freshly made solutions were utilized to prevent any contamination.

Synthesis of oxadiazole dertivative: A mixture of naphthaldehyde (1.0 equiv.) and nicotinic hydrazine (1.0 equiv.) dissolved in 30 mL methanol was refluxed until the complete condensation was attained (monitored by TLC). Then, the subsequent solvent was evaporated using a rotary evaporator under reduced pressure and the residue was redissolved in 15 mL DMSO, then 3.0 equiv. of K_2CO_3 and 1.2 equiv. of I_2 were added successively (**Scheme-I**). Furthermore, the reaction mixture was stirred at 100 ºC (4 h) till the completion of the reaction. After cooling, the resulting mixture was treated with a 5% solution of $Na_2S_2O_3$ before being extracted with ethyl acetate. The organic layer was dried over anhydrous magnesium sulfate after washing it with NaCl solution. The resultant residue was recrystallized by column chromatography [25]. The final product was obtained as a white solid. ^{1}H NMR (400 MHz) δ ppm: 9.40 (dd, *J* = 2.2, 0.7 Hz), 9.27 (dd, *J* = 8.6, 0.7 Hz), 8.81 (dd, *J* = 4.9, 1.7 Hz), 8.51-8.45 (m), 8.28 (dt, *J* = 7.3, 3.7 Hz), 8.06 (d, *J* = 8.3 Hz), 7.95 (dt, *J* = 8.0, 4.1 Hz), 7.71 (ddd, *J* = 8.5, 7.3, 3.9 Hz), 7.64-7.57 (m), 7.51 (ddd, *J* = 8.0, 4.9, 0.8 Hz); HRMS (*m/z*) (M+H) calculated for $C_{17}H_{11}N_3O$ is 274.0973.

The chemical compositions of the acquired mild steel (MS) coupons were found as (by wt.%): Cr: 0.056; Cu: 0.010; Si: 0.015; Ti: 0.002; Ni: 0.009; S: 0.017; P: 0.019; Mo: 0.018; C: 0.054 and Fe: 99.8. The dimension of 0.42 mm thick coupons was 3.0 cm × 2.0 cm. To get mirror finishing, the specimens were rubbed with various grades SiC emery paper (320-2000) and then finally degreased with hexane and acetone. Furthermore, these specimens were washed with double distilled water and dried as per ASTM standard G-31 to provide a refined perspective of these tested coupons.

Corrosion measurements

Gravimetric analysis: The traditional gravimetric method was used to carry out weight loss studies. The obtained rectangular MS coupons were immersed in 30 mL 1M HCl for 24 h at 303 K with/without changing inhibitor concentrations (50 to 500 ppm). The corroded product was mechanically cleaned by abrasively scrubbed with a brush after the permitted immersion time, then washed with ethanol, hexane and acetone while being ultrasonically cleaned, followed by a final rinse with ultrapure water. The tested coupons were then removed. After drying in an oven at 100 ºC, the weight loss of these coupons was measured with an analytical balance (precision ± 0.1 mg). The same was repeated to calculate the average weight loss, corrosion rate (C_R) in mg cm^{-2} h^{-1}, inhibition efficiency (IE) and surface coverage (θ). Eqns. 1 and 2 were used to compute the C_R and IE, respectively [26-29].

$$C_R = \frac{\Delta W}{At} \quad (1)$$

where ΔW stands for weight loss in mg, A is the coupon's area in cm^2 and t is the submergimg time (h).

$$IE\ (\%) = \frac{W_o - W}{W_o} \times 100 \quad (2)$$

where W_o and W represent weight loss without/with inhibitors, respectively.

Furthermore, the IE (%) was calculated from C_R by utilizing the following equation:

$$IE\ (\%) = \frac{C_R^o - C_R}{C_R^o} \times 100 \quad (3)$$

where C_R^o and C_R are the corrosion rates in the non-existence and existence of different inhibitor concentrations.

The surface coverage (θ) can be correlated with corrosion rate as well as weight loss by the following equations:

$$\theta = \frac{C_R^o - C_R}{C_R^o} \quad (4)$$

or

$$\theta = \frac{W_o - W}{W_o} \quad (5)$$

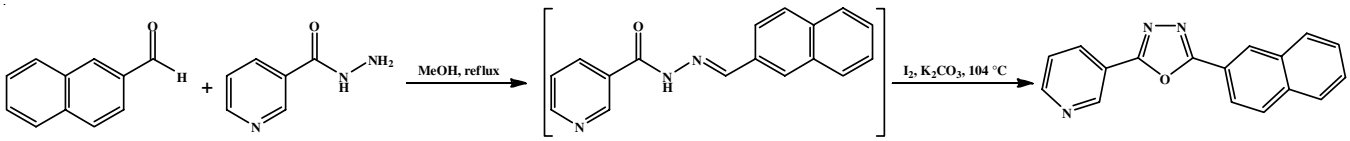

Scheme-I: Synthesis of 3-(5-naphthalen-2-yl-[1,3,4]oxadiazol-2-yl)pyridine (NOP)

Electrochemical evaluations: The electrochemical analysis of the synthesized NOP inhibitor has been carried out using Princeton Applied Research Parastat-4000. The EIS and PDP were accomplished by utilizing a three-electrode system that includes a silver electrode along with a luggin capillary as a reference electrode, a platinum electrode that functioned as the counter electrode and a rectangle-shaped MS sample coupon acting as a working electrode (with an exposed area of 1.0 cm^2). Each MS coupon was thoroughly cleaned before submerging. The corrosion potential ($-E_{corr}$) with a signal amplitude of 10 mV was employed to conduct EIS studies between 10 kHz and 0.01 Hz frequency for the investigated inhibitors (NOP) at four different concentrations ranging from 50 to 500 ppm.

The MS specimens were dipped in corrosive electrolyte for 60 min before the execution of EIS analysis to achieve a consistent corrosion potential and allow the open circuit potential (OCP) to stabilize. For polarization measurements, the anodic and cathodic curves were scanned between -250 mV and +250 mV (*vs.* silver electrode) at a scan rate of 1.0 mV/s. Electrochemical constraints such as corrosion potential (E_{corr}), corrosion current density (i_{corr}), anodic (β_a) and cathodic (β_c) Tafel slopes were calculated by extrapolation of Tafel slopes. I_{corr} was utilized to for IE calculation.

Morphological analysis: The surface morphology of MS specimens was recorded with the magnification of 1 µm before and after the specimens in 1M HCl (24 h) solution tested with and without inhibitors concentration of 500 ppm. The experiments were examined using a Zeiss Gemini SEM 500 Thermal Field Emission with a 15 kV acceleration beam.

Density functional theory (DFT) studies: The entire shape was optimized using DFT software and the $DMol^3$ module in the aqueous phase [30-34]. The energy gap (ΔE), the fraction of electron transmitted (ΔN) and the dipole moment (µ) were determined to correlate these descriptors of synthesized NOP in neutral forms with the effectiveness of their inhibition. The following equations and Koopman's theorem were used to compute several parameters, including ionization potential (IP), electron affinity (EA), electro-negativity (χ), hardness (η) and softness (σ).

$$EA = -E_{LUMO} \quad (6)$$

$$IP = -E_{HOMO} \quad (7)$$

$$\chi = \frac{IP + EA}{2} \quad (8)$$

$$\eta = \frac{IP + EA}{2} \quad (9)$$

$$\sigma = \frac{1}{\eta} \quad (10)$$

RESULTS AND DISCUSSION

Evaluation of inhibition efficiency

Gravimetric analysis: The effect of added NOP in 1M HCl solution was examined using gravimetric measurement after the requisite immersion period (24 h). Table-1 displays this study's characteristic parameters (C_R and IE). The findings made it evident that in 1M HCl environment, the NOP significantly impacted IE properties against MS corrosion. After 24 h, the inhibition performance reached its highest value of 92.57% at 500 ppm as the inhibitor concentration increased (Fig. 1). The corrosion rate was effectively reduced to as low as 0.25 mg cm^{-2} h^{-1}. The remarkable IE shown by the NOP can be attributed to the outstanding adsorption behaviour of pyridine, oxadiazole and benzene moieties, which develop a barrier on the MS surface and inhibit the corrosion process in aggressive acidic conditions.

TABLE-1
GRAVIMETRIC CALCULATIONS BEFORE AND AFTER THE NOP FOR MS IN 1M HCl

Inhibitor	Concentration (ppm)	C_R (mg cm^{-2} h^{-1})	η_{WL} (%)	θ
Blank	0	3.364	–	–
NOP	50	0.905	73.09	0.731
	100	0.710	78.89	0.789
	250	0.446	86.74	0.867
	500	0.250	92.57	0.926

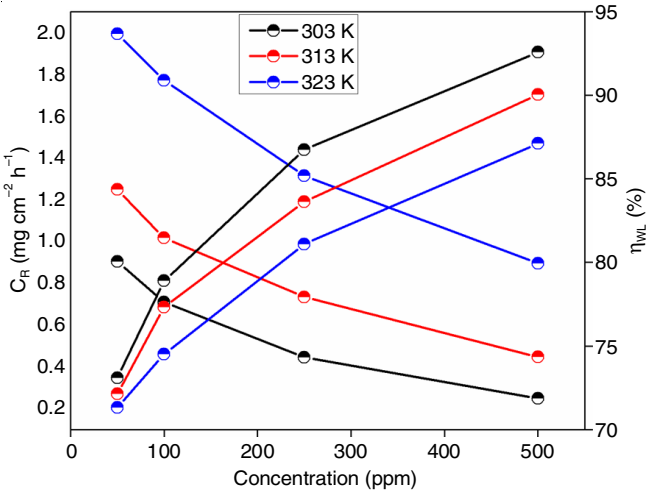

Fig. 1. Temperature-dependent inhibition efficiency and corrosion rate of NOP at varying concentrations of NOP

Potentiodynamic polarization (PDP) studies: The PDP analysis were performed by dipping the working electrode in 1M HCl solution for 60 min before being conducting the experiments (with/without inhibitor). Fig. 2 illustrates the outcomes of static polarization tests.

The polarization plots were used to assess all the relevant electrochemical kinetic parameters, including i_{corr}, E_{corr}, η% and β_a and β_c (anodic and cathodic slopes) (Table-2). These results were obtained by extrapolating Tafel slopes around the linearized current areas. The effective adsorption characteristics and the propensity of the NOP to produce a defensive film on the working electrode festinate its protective action [35-39]. Across all inhibitor concentrations, two linear segments were observed. In the limited polarization potential domain, the first segment shows a steady increase in current density, whereas the remaining segments show a rapid increase. After the investi-

TABLE-2
POTENTIODYNAMIC POLARIZATION VARIABLES FOR MILD STEEL CORROSION IN EXISTENCE AND NON-EXISTENCE OF NOP

Inhibitor	Concentration (ppm)	$-E_{corr}$ (mV*vs.* SCE)	i_{corr} (μAcm^{-2})	β_a (mV dec^{-1})	$-\beta_c$ (mV dec^{-1})	η_{PDP} (%)	θ
Blank	0	458.65	568.34	127.45	119.54	–	–
NOP	50	475.25	282.71	113.24	128.57	50.26	0.503
	100	486.54	144.54	104.45	131.47	74.57	0.746
	250	511.57	117.50	124.68	109.45	79.33	0.793
	500	532.25	102.84	137.98	101.74	80.15	0.802

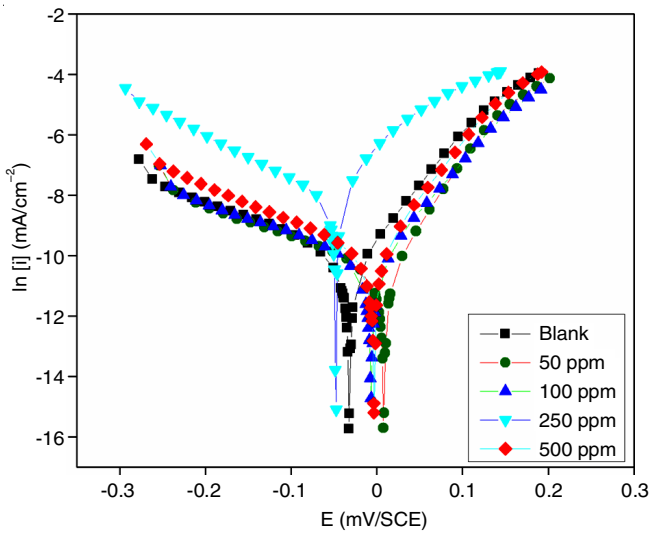

Fig. 2. Effect of addition of NOP on the PDP curves at different concentrations of NOP

gated inhibitor (NOP) was introduced to the corrosive solution, some changes were observed in the β_a and β_c.

The anodic branch's decrease in partial current was less significant than that of the cathodic unit. If the shift exceeds ±85 mV, the inhibitors were classified as cathodic or anodic and characterized as mixed-type inhibitors. As the E_{corr} value shift was less than 85 mV, the developed inhibitor in this current investigation displayed the mixed-type behaviour. The PDP data provide further details on the kinetics of cathodic and anodic processes. They are also congruent with the gravimetric measurement outcomes and give more information on the inhibitors' mechanism of action.

The IE can also be calculated from the corrosion current densities by the equation given below:

$$\eta_{Tafel}(\%) = \frac{i_R^o - i_R}{i_R^o} \times 100 \quad (11)$$

where i_R^o and i_R are the corrosion current density in the prior to and following the NOP.

EIS measurements: The interaction between the designed NOP and the electrode surface interface can be examined using EIS (charge transfer, diffusion and adsorption). Semicircle capacitance was observed across the whole frequency range (Nyquist curve, Fig. 3) for the MS coupons dipped in 1M HCl solution with/without additional inhibitor. As the inhibitor dose rises, semicircle's radius also rise accordingly. Due to the irregularity and frequency dispersion of the electrode surface, semicircle loops are likewise non-regular [40]. The Nyquist plot's findings were strengthened by Bode curves (Fig. 4). Furthermore, it is evaluated that the inhibitors' loop size is larger than that of the blank. This difference grows with inhibitor concentration due to the adsorptive protecting species occupying the MS surface [41].

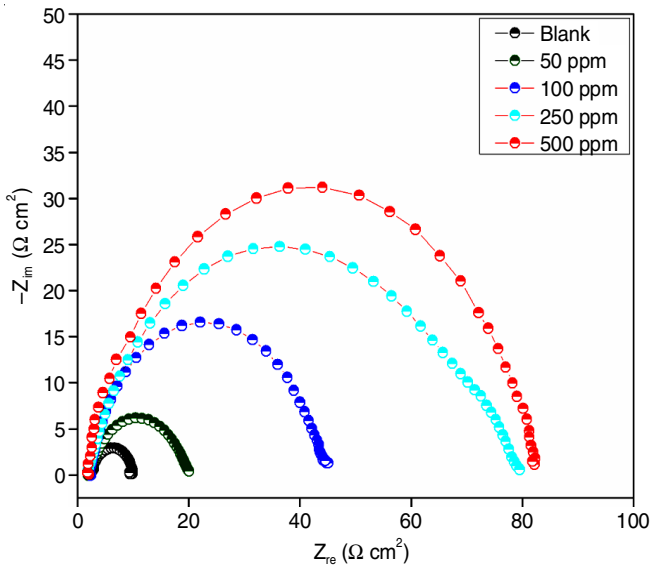

Fig. 3. Effect of addition of NOP on Nyquist plot for MS in 1M HCl solution

An electrochemical equivalent circuit (Fig. 5) containing a solution resistance (R_s), the constant phase element (CPE) as well as the charge transfer resistance (R_{ct}) (Table-3) was used to explain the impendence performance [42].

TABLE-3
EIS PARAMETERS FOR MILD STEEL CORROSION PRIOR TO AND FOLLOWING THE NOP

Inhibitor	Conc. (ppm)	R_{ct} ($\Omega.cm^2$)	(CPE/Yo) $\times 10^6$	η_{dl}	R_s (Ω)	R_p (Ω)	C_{dl} (μF cm^{-2})	η_{EIS} (%)	θ	χ^2
Blank	0	9.31	245.09	0.875	2.62	34.23	116.99	-		0.124
NOP	50	20.07	140.66	0.828	5.20	33.31	80.23	53.60	0.536	0.165
	100	44.57	134.72	0.790	5.29	39.07	41.59	79.10	0.791	0.177
	250	79.57	120.16	0.739	5.57	46.77	30.45	88.29	0.883	0.324
	500	81.86	105.94	0.664	5.64	56.09	24.70	88.62	0.886	0.248

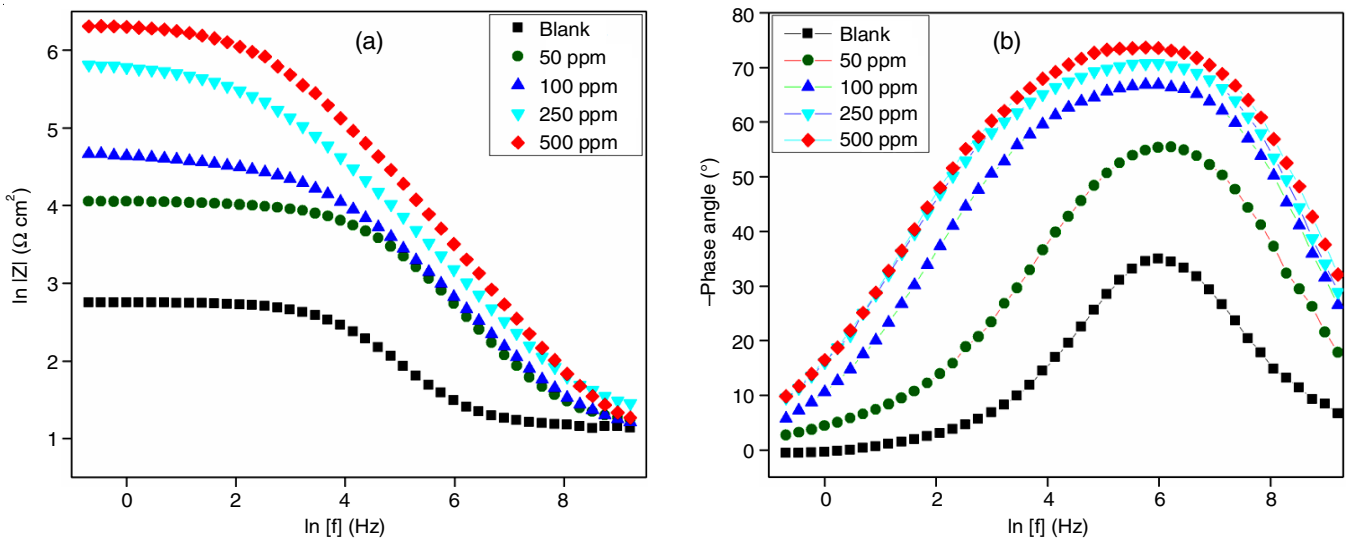

Fig. 4. (a) Bode plot and (b) phase angle plot for mild steel in 1M HCl solution for varying concentrations of NOP

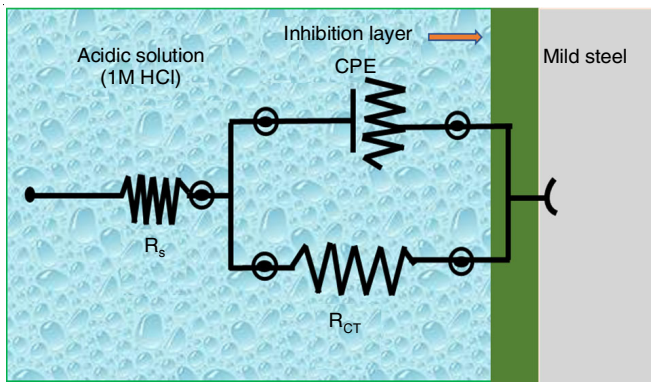

Fig. 5. Equivalent circuit used to fit EIS data

The CPE_{dl}, which offers more precise adjustment and can be used to assess the depressing nature of the semicircles [43], may be expressed as:

$$Z_{CPE} = Q^{-1} (i\omega)^{-n} \quad (12)$$

where, Q is used for the CPE constant, i and ω stand for imaginary roots and angular frequency, respectively, while n is the deviation indicator related to mild steel surface homogeneity. Furthermore, the formula given below can be utilized to calculate the double-layer capacitance (C_{dl}) [44,45]:

$$C_{dl} = \frac{1}{2\pi f_{max}} \times \frac{1}{R_{CT}} \quad (13)$$

where, f_{max} is the frequency on the top of the semicircle of Z_{real} axis and R_{CT} stands for the charge transfer resistance at various concentrations. η_{EIS} (%) was estimated by using the formula:

$$\eta_{EIS}(\%) = \frac{R_{CT} - R^{o}_{CT}}{R_{CT}} \times 100 \quad (14)$$

where, R_{CT} and R^{o}_{CT} denote the charge transfer resistances inclusion/exclusion of the inhibitor.

It is determined that NOP exhibits the highest R_{CT} value at 81.86 Ω cm^2. Additionally, it has been observed that the R_{CT} value for the inhibitor under study is congruent with the reduction in the double-layer capacitance (C_{dl}) (Table-3). This finding may be explained in terms of better surface coverage on the MS surface by the examined NOP obtained after replacing the H_2O and Cl^- ions [46]. Metal dissolution is decreased due to impending extra mass and electron charge density [47].

According to the Bode and phase angle plot (Fig. 4a-b), the adsorption phenomenon caused ln |z| and the phase angle approach to zero at the high-frequency region, which indicates that the electrolytic solution has high conductivities values. The improvement in total impedance seen with increasing inhibitor concentration in electrochemical experiments was consistent with the NOP's protective properties.

Adsorption studies: For analyzing the interaction between the adsorbed inhibitors, adsorption isotherms provide ample information. The surface coverage (θ) *vs.* conc. of the inhibitors (C_{inh}) was correlated using the Langmuir adsorption isotherm. After data evaluation, it was evaluated that the regression coefficient for the linear curve fitting caused by the Langmuir adsorption isotherm is 0.99628 (Fig. 6). Additionally, K_{ads} was calculated (eqn. 15) and correlated to ΔG^{o}_{ads} (standard free energy of the adsorption isotherm) by the following equality [48,49].

$$\Delta G^{o}_{ads} = -RT \ln(55.5 \times K_{ads}) \quad (15)$$

The physical adsorption will occur if the value of ΔG^{o}_{ads} is less negative than 20 kJ/mol; however, chemical adsorption behaviour was observed when is more negative than 40 kJ/mol [50,51]. In present work, the calculated value was found to be -29.782 kJ/mol (Table-4), demonstrating that NOP molecules physisorbed as well as chemisorbed on the MS and, as a result, firmly adsorbed to the metal surface.

Impacts of temperature and activation parameter: The temperature considerably impacts the behaviour of inhibitors and substrate in an aggressive medium. The ability of the MS to mitigate corrosion is decreased because the organic components become more soluble at higher temperatures. Gravimetric analysis was carried out at various concentrations of NOP at three different temperatures *viz.* 303, 313 and 323 K. Table-5

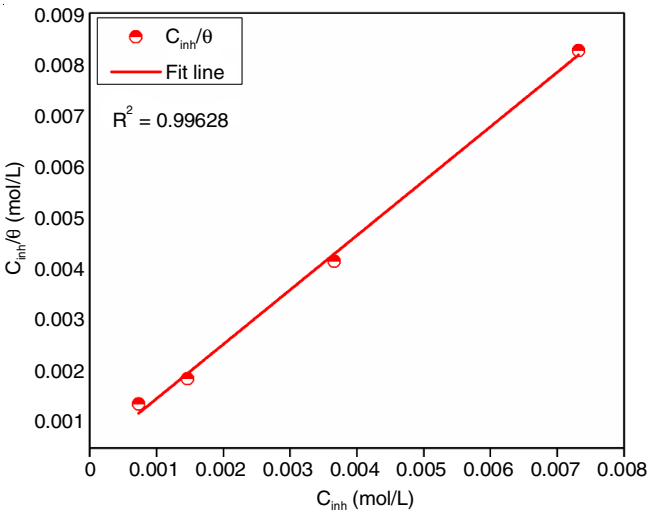

Fig. 6. Langmuir adsorption isotherms for NOP on mild steel in 1M HCl

TABLE-4
ADSORPTION PARAMETERS FOR NOP IN 1M HCl SOLUTION

Isotherm	Inhibitor	R^2	K_{ads}	ΔG°_{ads} (kJ/mol)
Langmuir	NOP	0.99628	2.46×10^3	-29.782

TABLE-5
C_R, IE (%) AND SURFACE COVERAGE (θ) OF MS IN 1M HCl SOLUTION OF NOP AT DIFFERENT TEMPERATURES

Temp. (K)	Conc. (ppm)	C_R (mg cm^{-2} h^{-1})	η_{WL} (%)	θ
Blank	0	3.364	–	–
303	50	0.905	73.09	0.731
	100	0.710	78.89	0.789
	250	0.446	86.74	0.867
	500	0.250	92.57	0.926
Blank	0	4.486	–	–
313	50	1.250	72.14	0.721
	100	1.017	77.33	0.773
	250	0.735	83.62	0.836
	500	0.447	90.04	0.900
Blank	0	6.951	–	–
323	50	1.993	71.33	0.713
	100	1.772	74.51	0.745
	250	1.314	81.09	0.811
	500	0.896	87.11	0.871

listed the rates of corrosion before and after exposure to various inhibitor doses.

The NOP's inhibitory effectiveness was shown to decrease and the corrosion rate grows with the temperature at different concentrations, indicating that the inhibition layer may disintegrate with the temperature rise (vide supra). The current investigation shows that Arrhenius-type behaviour is observed among the temperature and the corrosion rate. Applying eqn. 16 to various temperature ranges with and without NOP makes it easy to evaluate the E_a of the corrosion process [52,53].

$$\ln C_R = A - \frac{E_a}{RT} \quad (16)$$

The transition state theory was used to evaluate the corrosion process's thermodynamic parameters such as enthalpy (ΔH) and entropy (ΔS), whereas E_a was calculated from the slope of the equation ($-E_a/RT$) (Fig. 7).

$$C_R = \frac{RT}{Nh}\exp\left(\frac{\Delta S}{R}\right)\exp\left(\frac{-\Delta H}{RT}\right) \quad (17)$$

ΔH and ΔS were assessed from the plot of ln (CR/T) *vs.* 1/T (Fig. 8) and are presented in Table-6. The inhibited electrolytes have a higher activation energy than the uninhibited ones. The

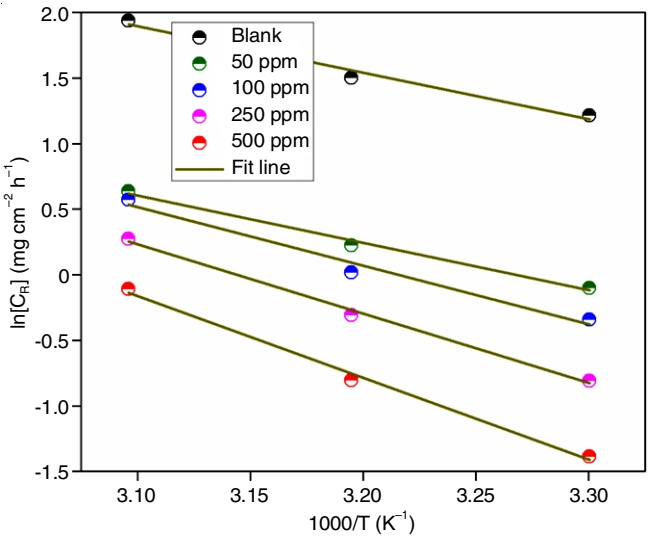

Fig. 7. ln [C_R] *versus* 1000/T at different concentrations of NOP

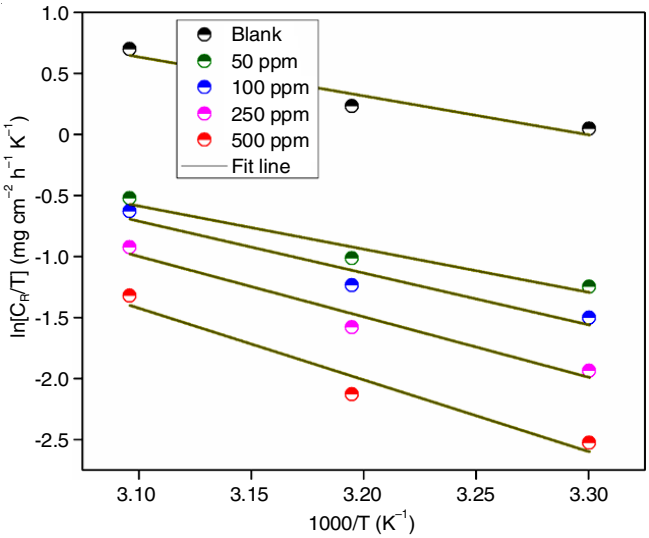

Fig. 8. ln [C_R/T] *versus* 1000/T for mild steel corrosion in 1M HCl solution at various concentrations of NOP

TABLE-6
MILD STEEL ACTIVATION PARAMETERS
(E_a, ΔH, ΔS) FOR MILD STEEL WITH/WITHOUT NOP

Medium	Conc. (ppm)	E_a (kJ/mol)	ΔH (kJ/mol)	ΔS (J mol^{-1} K^{-1})
Blank	0	29.45	26.49	-111.36
NOP	50	29.95	29.36	-110.13
	100	37.13	35.26	-94.13
	250	43.92	41.15	-78.27
	500	51.82	48.82	-58.04

blank solution has an activation energy of 29.45 KJ/mol, whereas the activation energies varied from 51.82 to 29.95 KJ/mol for the inhibited solutions.

The inhibitory molecules in the electrolytic solution appear to act as a barrier against these corrosion reactions. It is further supported by the fact that the electrostatic contact between the MS and the inhibitory molecules is responsible for the rise in activation energy in this process [54]. The positive value of ΔH also indicates that the metal-dissolving process exhibits endothermic activity. Additionally, given that the E_a is higher than the enthalpy of their analogs, it is evident that the corrosion phenomena involves a gaseous reaction brought on by proton reduction [55]. Furthermore, the negative values of ΔS show a decrease in randomness [56]. The reaction involves the activated complexes formation, which is the slow step and hence the rate determining step.

Surface characterization: An efficient method for corroborating the findings of gravimetric and electrochemical tests is to examine the morphological analysis of the MS surface after polishing (with 320-2000 grade SiC emery paper) and immersion in 1M HCl electrolyte in the inclusion and exclusion of the investigated inhibitors. The FESEM images show that after being submerged for 24 h, the tested inhibitors dveloped a defensive film on the MS surface (Fig. 9). The acidic circumstances significantly corroded the MS surface, facilitating the tested coupons' rapid dissolution. As shown in Fig. 9, the unconstrained sample is rough and highly porous with very deep holes. Additionally, a significant amount of NOP was adsorbed on the MS surface, slowing down the metal dissolution process.

DFT calculations: Quantum chemical investigations, which are astounding and instructive methodologies, can be used to evaluate and comprehend the structural information of organic compounds that trigger the corrosion rate and have inhibitory characteristics [56-58]. To understand the corrosion protection system of applied molecules in terms of molecular and electronic characteristics [59-68], the DFT parameters *viz.* E_{HOMO}, E_{LUMO}, energy gap (ΔE) and dipole moment (μ) were computed. The HOMO-LUMO energy levels and the chemical reactivity of the inhibitor are directly correlated, as shown by FMOs. Table-7 indicates that NOP has greater E_{HOMO} and relatively lower E_{LUMO} values due to their capacity to donate electrons to the metal's empty *d*-orbital and their propensity to accept them by back donation, supporting the inhibitors' potent adsorption activity.

Another important parameter that gives information on the bond polarity and the dispersal of electrons in the molecule is the dipole moment (μ) [69-71]. The higher value of μ helps to increase the inhibitory efficiencies by enhancing the adsorption characteristics. The amount of solvation energy of a molecule in water is determined by its dipole moment, which also displays the relative propensity of molecule to stick to the surface of water. Another factor affecting the adsorption behaviour of the inhibitors and chemical relativities is the degree of softness and hardness of the inhibitors. The following equation can be used to compute and correlate the electron affinity and ionization energy.

$$\eta = \frac{I - A}{2} \tag{18}$$

where η denotes the degree of hardness and softness (σ) is the inverse of hardness. Softer molecules have a smaller energy gap between the HOMO and LUMO. As a result, they exhibit higher chemical reactivity and greater corrosion inhibitor capabilities since they can quickly transfer the electron to the acceptor (Fig. 10).

Additionally, the electron transfer (ΔN) value also comprehends the interaction between metal and inhibitory molecules [72], which is calculated as:

$$\Delta N = \frac{\varphi_{Fe} - \chi_{inh}}{2(\eta_{Fe} + \eta_{inh})} \tag{19}$$

According to DFT calculations, the calculated value of φ was observed to be 4.82 eV for Fe (110). In present study, ΔN values are in accordance with the experimental outcomes. The total charge density of the investigated corrosion inhibitor (Fig. 11) is spread in major surrounding regions. This contains several

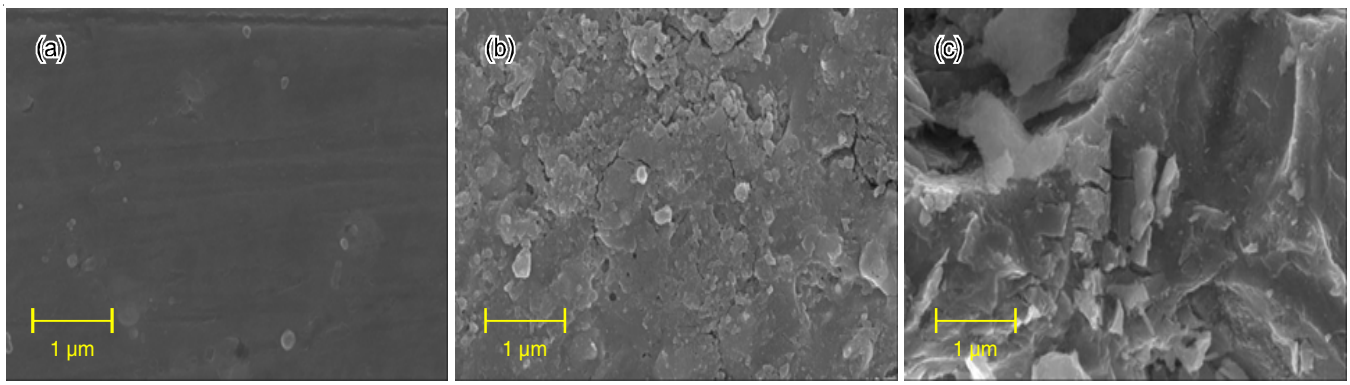

Fig. 9. (a) FESEM image of polished MS, (b) MS immersed in 1M HCl + 500 ppm NOP, (c) MS submerged in 1M HCl solution

TABLE-7
QUANTUM CHEMICAL DESCRIPTORS FOR NOP

Inhibitors	E_{HOMO} (eV)	E_{LUMO} (eV)	ΔE	I (eV)	EA (eV)	μ (D)	χ (eV)	η (eV)	σ (eV^{-1})	ΔN_{110}
NOP	-0.236	-0.087	0.149	0.236	0.087	5.760	0.074	0.161	13.984	0.183

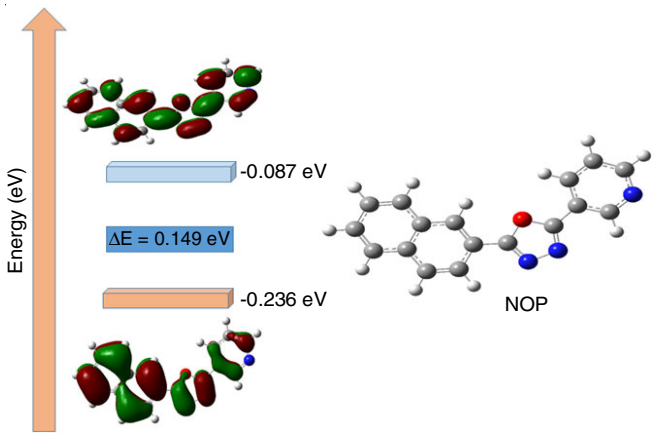

Fig. 10. Optimized geometries, HOMO and LUMO of investigated NOP

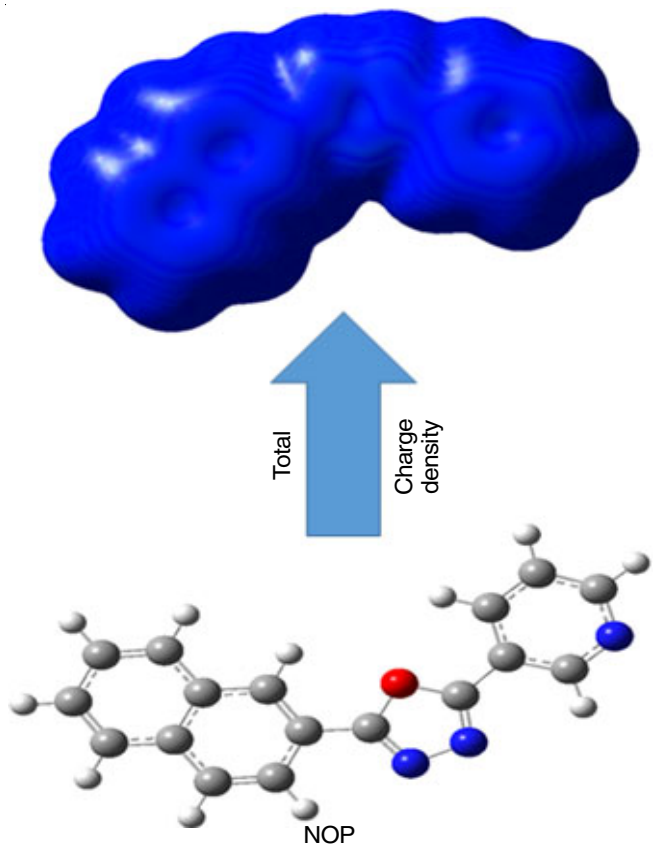

Fig. 11. Total charge density of NOP

functional groups that can interact with metal surfaces, forming a protective film that prevents or slows down the corrosion processby enhancing its adsorption and interaction with metal surfaces.

Molecular electrostatic potential (MEPs) studies: The electrophilic character in the NOP inhibitor is situated around the oxygen atom, that appears as red-yellow (Fig. 12). Due to their potent inhibitory effects, the electrophilic prone areas may increase the electron transmission with vaccant *d*-orbitals of Fe and so efficiently bind to the substrate (vide supra).

In Fig. 13, the surface contour of NOP has been illustrated. As can be seen, there is a huge affinity for the interaction towards the MS surface in aromatic rings, heteroatoms and several functional moieties, which facilitate effective adsorption on the MS surface and offer excellent corrosion inhibition. Overall, surface contour studies in DFT can provide valuable insights into the molecular-level interactions between corrosion inhibitors and metal surfaces, helping to guide the design of more effective inhibitors for corrosion prevention.

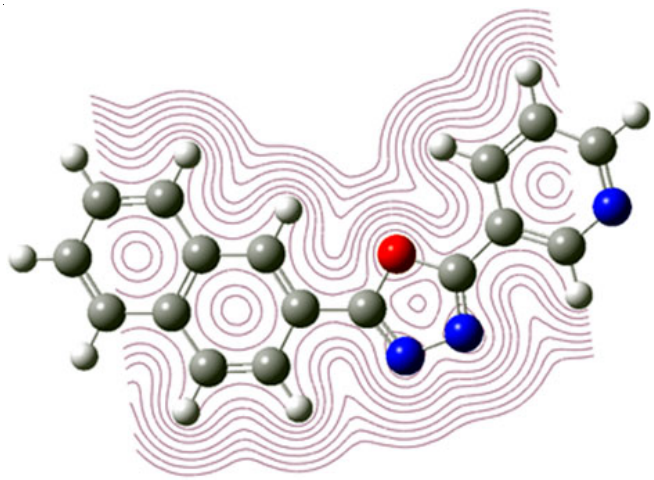

Fig. 13. Surface contour studies of NOP

Mechanism of anti-corrosive action: The results of numerous corrosion investigations (gravimetric analysis, EIS, PDP and DFT) suggested that adsorption behaviour is existing between the MS surface and the investigated inhibitors (Fig. 14). Furthermore, NOP is characterized primarily by their ease of protonation in acidic media [73]. In corrosive media, heteroatoms like N and O are more likely to protonate. In the meantime, it is observed that the chloride ion, preferentially absorbed on the MS surface electrostatically attracts the protonated NOP. In the adsorption process, the initial stage is physisorption, which is the basic step prior to chemical adsorption after which NOP makes an interaction through acceptor-donor liaison. The lone pair present on the N and O atoms is readily available for donation to empty *d*-orbital of Fe, demonstrating the chemical adsorption.

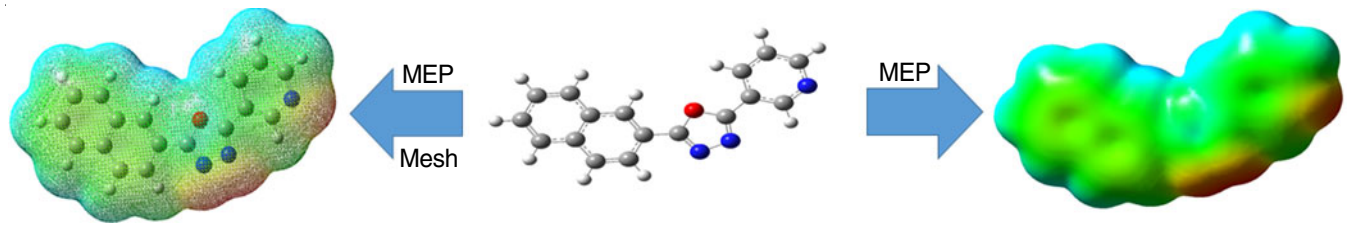

Fig. 12. MEP of the developed NOP

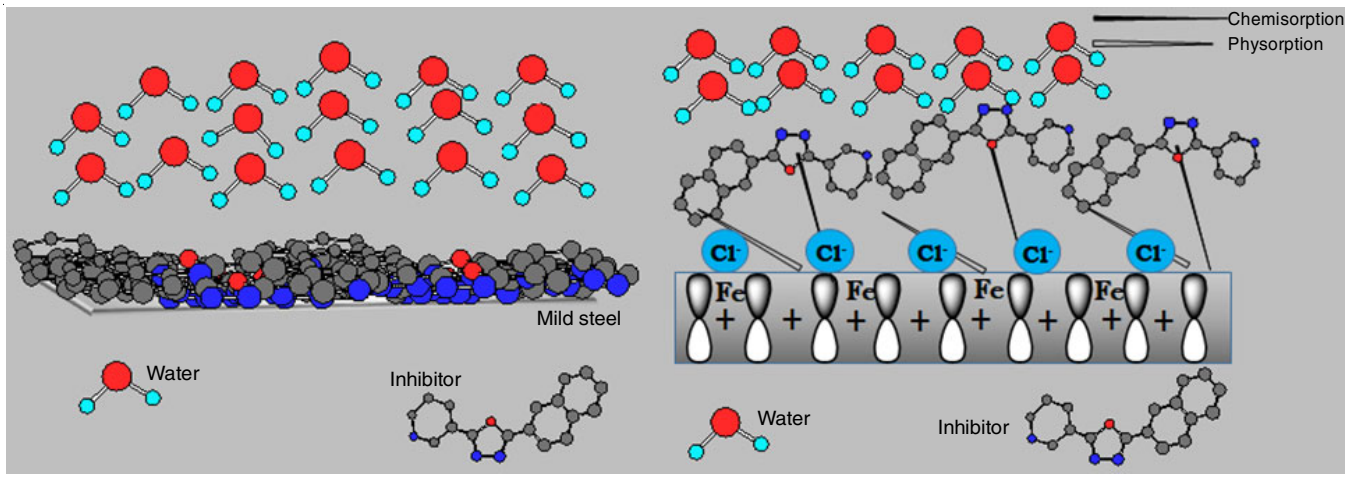

Fig. 14. Pictorial arcitecture of the NOP adsorption on mild steel in 1M HCl

Conclusion

The effective inhibitory performance of the newly synthesized oxadiazole dertivative 3-(5-naphthalen-2-yl-[1,3,4]-oxadiazol-2-yl)pyridine (NOP) of mild steel (MS) corrosion in 1M HCl was evaluated using systematic experimental and theoretical methodologies. The results indicated that the synthesized NOP inhibitor has outstanding inhibitory efficacy against MS corrosion. Its addition gradually decreased the corrosion current density, illustrated by PDP curves, indicating their mixed-type inhibitory activity. Additionally, these outcomes are supported by the EIS data. Langmuir adsorption isotherm was utilized to gather information about the adsorption phenomena was obtained. The SEM and DFT results showed that NOP displayed excellent adsorption behaviour on the mild steel surfaces. By increasing the activation energy, the studied inhibitor lowers the energy barrier for reactions involved in the corrosion process. The effectiveness of inhibitory performance agrees well with quantum mechanical characteristics such as $E_{LUMO,}$ dipole moment (μ), total energy (ΔE) of the system and the number of electrons transferred (ΔN) by these inhibitors. The results of this investigation have important implications for future efforts to improve corrosion inhibitors by functionalizing NOP.

ACKNOWLEDGEMENTS

One of the authors, DS is grateful to the CSIR, New Delhi, for the partial support as Senior Research Fellowship (File no.09/1063(0020)/2019-EMR-I). The authors also express their sincere gratitude to DCRUST, Murthal, India for providing the necessary research facilities.

CONFLICT OF INTEREST

The authors declare that there is no conflict of interests regarding the publication of this article.

REFERENCES

1. A.S. Algaber, E.M. El-Nemma and M.M. Saleh, *Mater. Chem. Phys.*, **86**, 26 (2004); https://doi.org/10.1016/j.matchemphys.2004.01.040
2. S.K. Mandal, Steel Metallurgy: Properties, Specifications and Applications, McGraw-Hill Education (2015).
3. I. Nadi, M. Bouanis, F. Benhiba, K. Nohair, A. Nyassi, A. Zarrouk, C. Jama and F. Bentiss, *J. Mol. Liq.*, **342**, 116958 (2021); https://doi.org/10.1016/j.molliq.2021.116958
4. D. Dwivedi, K. Lepková and T. Becker, *RSC Adv.*, **7**, 4580 (2017); https://doi.org/10.1039/C6RA25094G
5. K. Wan, P. Feng, B. Hou and Y. Li, *RSC Adv.*, **6**, 77515 (2016); https://doi.org/10.1039/C6RA12975G
6. F. Bentiss, M. Lagrenee, M. Traisnel, B. Mernari and H. Elattari, *J. Appl. Electrochem.*, **29**, 1073 (1999); https://doi.org/10.1023/A:1003421111890
7. T.Y. Soror, H.A.E. Dahan and N.G.E. Sayed Ammer, *J. Mater. Sci. Technol.*, **15**, 559 (1999).
8. F.E.-T. Heakal and A.E. Elkholy, *J. Mol. Liq.*, **230**, 395 (2017); https://doi.org/10.1016/j.molliq.2017.01.047
9. R. Ammal P, A. R Prasad, R. K, S. John and A. Joseph, *J. Adhes. Sci. Technol.*, **33**, 2227 (2019); https://doi.org/10.1080/01694243.2019.1637169
10. M. Aliofkhazraei, Developments in Corrosion Protection, pp. 710, Intech Open (2014).
11. S. Hooshmand Zaferani, M. Sharifi, D. Zaarei and M.R. Shishesaz, *J. Environ. Chem. Eng.*, **1**, 652 (2013); https://doi.org/10.1016/j.jece.2013.09.019
12. B.N. Popov, Corrosion Engineering: Principles and Solved Problems Book, Elsevier (2015).
13. J.K. Bangia, M. Singh, H. Om, K. Behera and M. Gulia, *J. Mol. Liq.*, **225**, 758 (2017); https://doi.org/10.1016/j.molliq.2016.11.002
14. N. Kumari, M. Singh, H. Om, K.M. Sachin and M. Pal, *J. Mol. Liq.*, **288**, 111043 (2019); https://doi.org/10.1016/j.molliq.2019.111043
15. N. Kumari, M. Singh, H. Om, K.M. Sachin and D. Sharma, *J. Mol. Liq.*, **305**, 112744 (2020); https://doi.org/10.1016/j.molliq.2020.112744
16. A.A. Rahim, E. Rocca, J. Steinmetz, M.J. Kassim, R. Adnan and M.S. Ibrahim, *Corros. Sci.*, **49**, 402 (2007); https://doi.org/10.1016/j.corsci.2006.04.013
17. W. Li, Q. He, C. Pei and B. Hou, *Electrochim. Acta*, **52**, 6386 (2007); https://doi.org/10.1016/j.electacta.2007.04.077
18. F. Bentiss, M. Traisnel, H. Vezin and M. Lagrenée, *Corros. Sci.*, **45**, 371 (2003); https://doi.org/10.1016/S0010-938X(02)00102-6
19. M. Lagrenée, B. Mernari, N. Chaibi, M. Traisnel, H. Vezin and F. Bentiss, *Corros. Sci.*, **43**, 951 (2001); https://doi.org/10.1016/S0010-938X(00)00076-7
20. D. Sharma, H. Om and A.K. Sharma, *Crit. Rev. Anal. Chem.*, (2022); https://doi.org/10.1080/10408347.2022.2080494
21. M. Lebrini, F. Bentiss, H. Vezin and M. Lagrenée, *Appl. Surf. Sci.*, **252**, 950 (2005); https://doi.org/10.1016/j.apsusc.2005.01.160

22. A.Y.I. Rubaye, H.T. Abdulsahib and A.A. Abdulwahid, *J. Encapsul. Adsorpt. Sci.*, **5**, 155 (2015); https://doi.org/10.4236/jeas.2015.53013
23. V. Kalia, P. Kumar, S. Kumar, P. Pahuja, G. Jhaa, S. Lata and H. Dahiya, *J. Mol. Liq.*, **313**, 113601 (2020); https://doi.org/10.1016/j.molliq.2020.113601
24. V. Kalia, P. Kumar, S. Kumar, M. Goyal, P. Pahuja, G. Jhaa, S. Lata, H. Dahiya, S. Kumar, A. Kumari and C. Verma, *J. Mol. Liq.*, **348**, 118021 (2022); https://doi.org/10.1016/j.molliq.2021.118021
25. W. Yu, G. Huang, Y. Zhang, H. Liu, L. Dong, X. Yu, Y. Li and J. Chang, *J. Org. Chem.*, **78**, 10337 (2013); https://doi.org/10.1021/jo401751h
26. D.K. Singh, S. Kumar, G. Udayabhanu and R.P. John, *J. Mol. Liq.*, **216**, 738 (2016); https://doi.org/10.1016/j.molliq.2016.02.012
27. M.A. Bedair, A.M. Abuelela, M. Alshareef, M. Owda and E.M. Eliwa, *RSC Adv.*, **13**, 186 (2022); https://doi.org/10.1039/D2RA05939H
28. I.B. Obot, E.E. Ebenso and Z.M. Gasem, *Int. J. Electrochem. Sci.*, **7**, 1997 (2012).
29. M.A. Bedair, H.M. Elaryian, E.S. Gad, M. Alshareef, A.H. Bedair, R.M. Aboushahba and A.E.-A.S. Fouda, *RSC Adv.*, **13**, 478 (2022); https://doi.org/10.1039/D2RA06574F
30. H. Rahmani, K.I. Alaoui, K.M. Emran, A. El Hallaoui, M. Taleb, S. El Hajji, B. Labriti, E. Ech-chihbi, B. Hammouti and F. El-Hajjaji, (2019); https://doi.org/10.20944/preprints201803.0116.v1
31. F. Benhiba, H. Serrar, R. Hsissou, A. Guenbour, A. Bellaouchou, M. Tabyaoui, S. Boukhris, H. Oudda, I. Warad and A. Zarrouk, *Chem. Phys. Lett.*, **743**, 137181 (2020); https://doi.org/10.1016/j.cplett.2020.137181
32. M. El Faydy, F. Benhiba, B. Lakhrissi, M.E. Touhami, I. Warad, F. Bentiss and A. Zarrouk, *J. Mol. Liq.*, **295**, 111629 (2019); https://doi.org/10.1016/j.molliq.2019.111629
33. T. Laabaissi, F. Benhiba, Z. Rouifi, M. Missioui, K. Ourrak, H. Oudda, Y. Ramli, I. Warad, M. Allali and A. Zarrouk, *Int. J. Corros. Scale Inhib.*, **8**, 241 (2019); https://doi.org/10.17675/2305-6894-2019-8-2-6
34. H.C. Andersen, *J. Chem. Phys.*, **72**, 2384 (1980); https://doi.org/10.1063/1.439486
35. F. Bentiss, M. Outirite, M. Traisnel, H. Vezin, M. Lagrenée, B. Hammouti, S.S. Al-Deyab and C. Jama, *Int. J. Electrochem. Sci.*, **7**, 1699 (2012).
36. F. El-Taib Heakal, N.S. Tantawy and O.S. Shehata, *Int. J. Hydrogen*, **24**, 19219 (2012); https://doi.org/10.1016/j.ijhydene.2012.10.037
37. J. Haque, V. Srivastava, C. Verma and M.A. Quraishi, *J. Mol. Liq.*, **225**, 848 (2017); https://doi.org/10.1016/j.molliq.2016.11.011
38. A. Salhi, S. Tighadouini, M. El-Massaoudi, M. Elbelghiti, S. Radi, A. Bouyanzer, S. El Barkany, F. Bentiss and A. Zarrouk, *J. Mol. Liq.*, **248**, 340 (2017); https://doi.org/10.1016/j.molliq.2017.10.040
39. H. Ouici, M. Tourabi, O. Benali, C. Selles, C. Jama, A. Zarrouk and F. Bentiss, *J. Electroanal. Chem.*, **803**, 125 (2017); https://doi.org/10.1016/j.jelechem.2017.09.018
40. A. Khadiri, A. Ousslim, K. Bekkouche, A. Aouniti, I. Warad, A. Elidrissi, B. Hammouti, F. Bentiss, M. Bouachrine and A. Zarrouk, *J. Bio Tribocorros.*, **4**, 64 (2018); https://doi.org/10.1007/s40735-018-0179-3
41. C. Jeyaprabha, S. Sathiyanarayanan, K.L.N. Phani and G. Venkatachari, *Appl. Surf. Sci.*, **252**, 966 (2005); https://doi.org/10.1016/j.apsusc.2005.01.098
42. C. Pan, Y. Song, W. Jin, Z. Qin, S. Song, W. Hu and D.H. Xia, *Trans. Tianjin Univ.*, **26**, 135 (2020); https://doi.org/10.1007/s12209-020-00238-8
43. F. Zhang, Y. Tang, Z. Cao, W. Jing, Z. Wu and Y. Chen, *Corros. Sci.*, **61**, 1 (2012); https://doi.org/10.1016/j.corsci.2012.03.045
44. D. Daoud, T. Douadi, S. Issaadi and S. Chafaa, *Corros. Sci.*, **79**, 50 (2014); https://doi.org/10.1016/j.corsci.2013.10.025
45. Y. El, *J. Mater. Environ. Sci.*, **7**, 371 (2016).
46. E. McCafferty and N. Hackerman, *J. Electrochem. Soc.*, **119**, 146 (1972); https://doi.org/10.1149/1.2404150
47. F. Growcock and R.J. Jasinski, *J. Electrochem. Soc.*, **136**, 2310 (1989); https://doi.org/10.1149/1.2097847
48. D. Benhmamou, M.R. Aouad, R. Salghi, A. Zarrouk, M. Assouag, O. Benali, M. Messali, H. Zarrok and B. Hammouti, *J. Chem. Pharm. Res.*, **4**, 3489 (2012).
49. H. Om, G.A. Baker, F.V. Bright, K.K. Verma and S. Pandey, *Chem. Phys. Lett.*, **450**, 156 (2007); https://doi.org/10.1016/j.cplett.2007.10.101
50. A. Nahle, F. El-Hajjaji, A. Ghazoui, N.E. Benchat, M. Taleb, R. Saddik, A. Elaatiaoui, M. Koudad and B. Hammouti, *Anti-Corros. Methods Mater.*, **65**, 87 (2018); https://doi.org/10.1108/ACMM-03-2017-1769
51. H. Rahmani, K.I. Alaoui, M.E. Azzouzi, F. Benhiba, A.E. Hallaoui, Z. Rais, M. Taleb, A. Saady, B. Labriti, A. Aouniti and A. Zarrouk, *Chem. Data Coll.*, **24**, 100302 (2019); https://doi.org/10.1016/j.cdc.2019.100302
52. E. Garcia-Ochoa, S.J. Guzmán-Jiménez, J.G. Hernández, T. Pandiyan, J.M. Vásquez-Pérez and J. Cruz-Borbolla, *J. Mol. Struct.*, **1119**, 314 (2016); https://doi.org/10.1016/j.molstruc.2016.04.057
53. A. Khadraoui, A. Khelifa, M. Hadjmeliani, R. Mehdaoui, K. Hachama, A. Tidu, Z. Azari, I.B. Obot and A. Zarrouk, *J. Mol. Liq.*, **216**, 724 (2016); https://doi.org/10.1016/j.molliq.2016.02.005
54. M.H. Sliem, M. Afifi, A. Bahgat Radwan, E.M. Fayyad, M.F. Shibl, F.E.T. Heakal and A.M. Abdullah, *Sci. Rep.*, **9**, 2319 (2019); https://doi.org/10.1038/s41598-018-37254-7
55. E.A. Noor, *Int. J. Electrochem. Sci.*, **2**, 996 (2007).
56. M.K. Sharma, S. Parashar, M. Chahal, K. Lal, N.U. Pandya and H. Om, *J. Mol. Struct.*, **1257**, 132632 (2022); https://doi.org/10.1016/j.molstruc.2022.132632
57. S. Abrishami, R. Naderi and B. Ramezanzadeh, *Appl. Surf. Sci.*, **457**, 487 (2018); https://doi.org/10.1016/j.apsusc.2018.06.190
58. H. Zhao, X. Zhang, L. Ji, H. Hu and Q. Li, *Corros. Sci.*, **83**, 261 (2014); https://doi.org/10.1016/j.corsci.2014.02.023
59. A. Thakur, A. Kumar, S. Kaya, R. Marzouki, F. Zhang and L. Guo, *Coatings*, **12**, 1459 (2022); https://doi.org/10.3390/coatings12101459
60. A. Kumar and A. Thakur, eds.: S. Rajendran, T.A. Nguyen, S. Kakooei, M. Yeganeh, Y. Li, Encapsulated Nanoparticles in Organic Polymers for Corrosion Inhibition, in: Corrosion Protection at the Nanoscale, Chap. 18, pp. 345–362 (2020); https://doi.org/10.1016/B978-0-12-819359-4.00018-0
61. A. Thakur, S. Kaya, A.S. Abousalem and A. Kumar, *Exp. Sustain. Chem. Pharm.*, **29**, 100785 (2022); https://doi.org/10.1016/j.scp.2022.100785
62. A. Thakur, A. Kumar, S. Sharma, R. Ganjoo and H. Assad, *Mater. Today Proc.*, **66**, 609 (2022); https://doi.org/10.1016/j.matpr.2022.06.479
63. A. Thakur and A. Kumar, *J. Bio. Tribocorros.*, **7**, 1 (2021); https://doi.org/10.1007/s40735-021-00501-y
64. A. Thakur, S. Kaya and A. Kumar, *Curr. Nanosci.*, **18**, 203 (2022); https://doi.org/10.2174/1573413717666210216120741
65. F. Bentiss, B. Mernari, M. Traisnel, H. Vezin and M. Lagrenée, *Corros. Sci.*, **53**, 487 (2011); https://doi.org/10.1016/j.corsci.2010.09.063
66. I.B. Obot and Z.M. Gasem, *Corros. Sci.*, **83**, 359 (2014); https://doi.org/10.1016/j.corsci.2014.03.008
67. D.H. Xia, C. Pan, Z. Qin, B. Fan, S. Song, W. Jin and W. Hu, *Prog. Org. Coat.*, **143**, 105638 (2020); https://doi.org/10.1016/j.porgcoat.2020.105638
68. F. Bentiss, F. Gassama, D. Barbry, L. Gengembre, H. Vezin, M. Lagrenée and M. Traisnel, *Appl. Surf. Sci.*, **252**, 2684 (2006); https://doi.org/10.1016/j.apsusc.2005.03.231
69. I.B. Obot and N.O. Obi-Egbedi, *Corros. Sci.*, **52**, 657 (2010); https://doi.org/10.1016/j.corsci.2009.10.017
70. N. Kumari, M. Singh, H. Om and K.M. Sachin, *RSC Adv.*, **9**, 12507 (2019); https://doi.org/10.1039/C9RA00728H
71. G. Gao and C. Liang, *Electrochim. Acta*, **52**, 4554 (2007); https://doi.org/10.1016/j.electacta.2006.12.058
72. A. Kokalj, *Electrochim. Acta*, **56**, 745 (2010); https://doi.org/10.1016/j.electacta.2010.09.065
73. R. Yildiz, T. Dogan and I. Dehri, *Corros. Sci.*, **85**, 215 (2014); https://doi.org/10.1016/j.corsci.2014.04.017